Grid supporting nonlinear control for AC-coupled DC Microgrids

Ömer Ekin, Filipe Perez, Friedrich Wiegel, Veit Hagenmeyer, Gilney Damm

Grid supporting nonlinear control for AC-coupled DC Microgrids

1st Ömer Ekin
Institute for Automation and Applied Informatics
Karlsruhe Institute of Technology (KIT)
Karlsruhe, Germany

2nd Filipe Perez
Supergrid Institute
Lyon, France

3rd Friedrich Wiegel
Institute for Automation and Applied Informatics
Karlsruhe Institute of Technology (KIT)
Karlsruhe, Germany

4th Veit Hagenmeyer
Institute for Automation and Applied Informatics
Karlsruhe Institute of Technology (KIT)
Karlsruhe, Germany

5th Gilney Damm
COSYS-IMSE Laboratory
University Gustave Eiffel
Marne-la-Vallée, France

2024 IEEE Sixth International Conference on DC Microgrids (ICDCM) | 979-8-3503-6363-0/24/$31.00 ©2024 IEEE | DOI: 10.1109/ICDCM60322.2024.10664838

***Abstract*—Direct Current (DC) Microgrids have risen as a good option for better integrating distributed renewable energies and various highly dynamic DC loads, such as electrical vehicle supply equipment or industrial grids. However, for the large-scale deployment of such DC Microgrids, developing enhanced control strategies for these inverter-based, highly dynamic grids is crucial. The present paper introduces an innovative nonlinear control tailored for DC Microgrids supporting Alternative Current (AC) grids. Building upon existing methods, we extend the nonlinear control paradigm by incorporating multiple batteries and an AC link. This integration not only bolsters support for the AC grid, but also enhances the stability of DC voltage. We validate the effectiveness of the proposed algorithm through experimental evaluations conducted on a Power Hardware-in-the-Loop (PHIL) DC Microgrid configuration and compare it to a cascaded PI controller based on a linearized model.**

***Keywords*—DC Microgrids, Distributed nonlinear control, Grid Support, DC Voltage Control**

I. Introduction

DC Microgrids have emerged as a promising solution for effectively integrating renewable energy sources, storage technologies, and power electronic-based loads. Their key advantages include fewer conversion steps, absence of skin effects, and reactive power, resulting in minimized energy losses and reduced copper requirements in transmission lines [1]. Consequently, DC Microgrids present a more environmentally friendly alternative to AC Microgrids [1]–[5]. An illustration of a DC Microgrid scheme is depicted in Fig. 1. Most of the components can be directly integrated into the DC Microgrid through a single converter. However, the implementation of DC Microgrids requieres the integration and control of a significant number of interconnected power converters, which presents a challenging task in practice. The best known and established control is the Proportional-Integral (PI) control, which often has a limited operating range, is very difficult to tune, and does not present a rigorous stability analysis, making nonlinear control more advantageous and usually better performing [6]–[9]. In additon, power converters in DC Microgrids typically behave like constant power loads, similar to negative impedances, and can cause instability, especially when using standard industrial PI controllers [10]–[12]. Therefore, it is crucial to develop customized nonlinear controllers to enhance stability [13], [14].

In [15] a nonlinear control is implemented to suppress large voltage/current transients in DC Microgrids. Feedback linearization techniques are proposed in [16] for system stability and robustness improvement. Singular perturbation analysis is used in [8], [17], [18] to ensure time-scale separation, which improves the control performance in DC/DC converter applications. In [4] a nonlinear controller implemented in Power Hardware-in-the-Loop (PHIL) for a special multi-terminal DC Microgrid is presented. This Microgrid serves as an apt representation of a residential district that includes local renewable energy generation, energy storage system and DC loads. The control scheme in [4] reduces the capacitance requirements of [11] and [19] and enhances robustness against system shutdowns triggered by fuses or breakers. In the present work, we extend the approach introduced in [4] to include multiple battery systems and an interface to the AC grid.

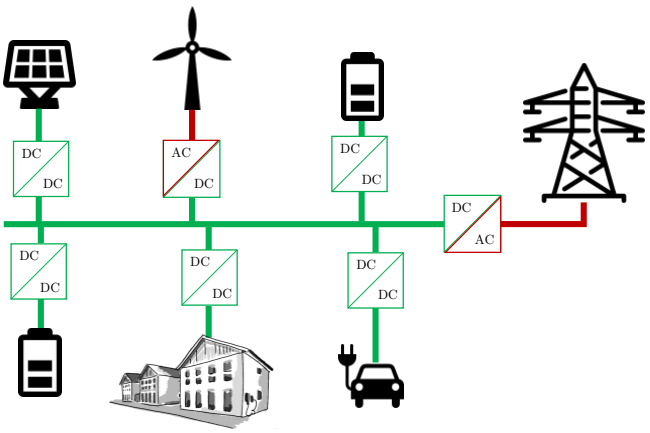

Fig. 1: An example DC Microgrid Scheme

This extension enables grid support and improves DC voltage stability through the use of a three-phase voltage source converter (VSC). The manifold contribution of the present work is to enable the following:

(1) AC coupling in the nonlinear control algorithm.
(2) Two batteries on the same DC bus.
(3) PHIL experimental validation of the extended method.

The remainder of the paper is organized as follows: In section II the DC Microgrid configuration and model are explained. The proposed control strategy is introduced in section III. The PHIL setup is presented in section IV. The performance of the proposed control strategy is demonstrated by real PHIL setup experiments in section V. Finally, a conclusion is given in section VI.

II. Microgrid Model

The established DC Microgrid composists of a photovoltaic (PV) system, two identical batteries, two load ports with different voltage levels, and a VSC, as shown in Fig. 2. In contrast to earlier methodologies [4], [20], the DC control is managed by the tandem operation of two batteries, complemented by the AC connection that allows grid-connected operation. The battery systems are chosen to be identical and controlled to stabilize the DC voltage at the point of common coupling (PCC). The PV emulator system is used as the main generation unit in the considered DC Microgrid. It is controlled by an incremental conductance algorithm to track the maximum power point (MPPT) [21], [22]. The DC load outputs are connected to resistive DC devices in the DC House of the Energy Lab [23]. The DC bus as the PCC is modeled as the interconnection of all subsystems. The model used for the DC side is consistent with that used in [4] and extended by adding an index i:

$$\dot{I}_{Bi} = \frac{V_{Bi}}{L_{Bi}} - \frac{R_{Bi}+R_{01}}{L_{Bi}} I_{Bi} - \frac{V_{C,Bi}}{L_{Bi}} u_{Bi} \tag{1}$$

$$\dot{V}_{C,Bi} = \frac{V_{DC}-V_{C,Bi}}{C_{Bi}R'_{Bi}} - \frac{V_{C,Bi}}{C_{Bi}R'_{Bi}} + \frac{I_{Bi}}{C_{Bi}} u_{Bi} \tag{2}$$

where V_{Bi} and I_{Bi} are the voltages and currents of the batteries, respectively. R_{Bi}, and R_{01} are the cable resistance of the battery and the MOSFETs losses. u_{Bi} is the duty cycle of the converter i. C_{Bi} and $V_{C,Bi}$ are the capacitor of the converter and the voltage on the capacitor, respectively. V_{DC} is the voltage on the DC bus.

The AC interconnection is modeled by the park-transformed dynamics of the VSC model:

$$\dot{I}_{l,d} = -\frac{R_l}{L_l} I_{l,d} + \omega I_{l,q} + \frac{V_{DC}}{2L_l} u_d - \frac{V_{l,d}}{L_l} \tag{3}$$

$$\dot{I}_{l,q} = -\frac{R_l}{L_l} I_{l,q} - \omega I_{l,d} + \frac{V_{DC}}{2L_l} u_q - \frac{V_{l,q}}{L_l}. \tag{4}$$

where $I_{l,d}$ and $I_{l,d}$ are the direct and quadratic output currents of the VSC, and $V_{l,d}$ and $V_{l,q}$ the direct and quadratic voltages on the AC line, respectively. L_l is the output inductance of the VSC and R_l the line resistance between the VSC and the AC grid. u_d and u_q are the direct and quadrature duty cycles obtained through the Park transformation of the three duty cycles of the three half-bridges, and vice versa. ω is the AC grid frequency.

III. Nonlinear control Method

In this chapter, PI-based control is introduced first, followed by nonlinear control. The control strategy involves different objectives for each component. For example, the batteries are to maintain a predefined reference voltage on the DC bus. The PV is supposed to track the maximum power injection, while the load converters are supposed to maintain the output voltage at a certain value. The VSC is controlled to follow a higher-level controller that provides active and reactive power references. Some references are fixed *a priori*, while others are provided by a higher tertiary-level controller, which is outside the scope of this work.

A. PI-based control

The PI-based control scheme is shown in Fig. 3. A cascaded PI is used for voltage and current control [24]. In addition, an anti-windup method is added to prevent integral windup, which occurs when the control signal saturates, by adjusting the integral action to maintain stability and performance.

B. Nonlinear Control

1) Control of the batteries: A feedback linearization method is used to design the control law for the battery subsystems. This control law is intended to control the current to a reference to be designed:

$$\begin{aligned} u_{Bi} &= \frac{1}{V_{C,Bi}} \left[L_{Bi}\phi_{Bi} - V_{Bi} + (R_{Bi}+R_{0i}) I_{Bi} \right] \\ \phi_{Bi} &= -K_{Bi}(I_{Bi} - I^*_{Bi}) - K^{\alpha}_{Bi}\alpha_{Bi} \\ \dot{\alpha}_{Bi} &= I_{Bi} - I^*_{Bi} \end{aligned} \tag{5}$$

where $i = [1, 2]$, α is the integral term, and I^*_{Bi} is the current reference.

The next step is to correctly compute the reference value I^*_{Bi} used as the control input such that $V_{C,Bi} \to V^*_{DC}$, since the resistance between $V_{C,Bi}$ and V^*_{DC} is very small, it can be neglected ($R'_{Bi} \sim 0$). Therefore, the boundary layer model of the DC bus is obtained from singular perturbation analysis [20]:

$$\begin{aligned} \dot{V}_{C,Bi} &= \frac{1}{R'_{Bi}C_{Bi}}(V_{DC} - V_{C,Bi}) + \\ &\quad + \frac{I^*_{Bi}}{C_{Bi}V_{C,Bi}} \left[V_{Bi} - (R_{Bi}+R_{0i}) I^*_{Bi} \right] \end{aligned} \tag{6}$$

where V_{DC} is the voltage measured at the common connection point of the converters in the DC Microgrid, and is considered a non-controlled variable. Applying feedback linearization, where $V_{C,Bi}$ is the control output, the relative degree is two. Consequently, one can find a proper control input ($\dot{I}^*_{Bi}$) in the second time-derivative of $V_{C,Bi}$ dynamics:

$$\dot{I}^*_{Bi} = \frac{1}{\mathcal{L}_{g_i}\mathcal{L}^1_{f_i}(V_{C,Bi})} \left[v_d - \mathcal{L}^2_{f_i}(V_{C,Bi}) \right] \tag{7}$$

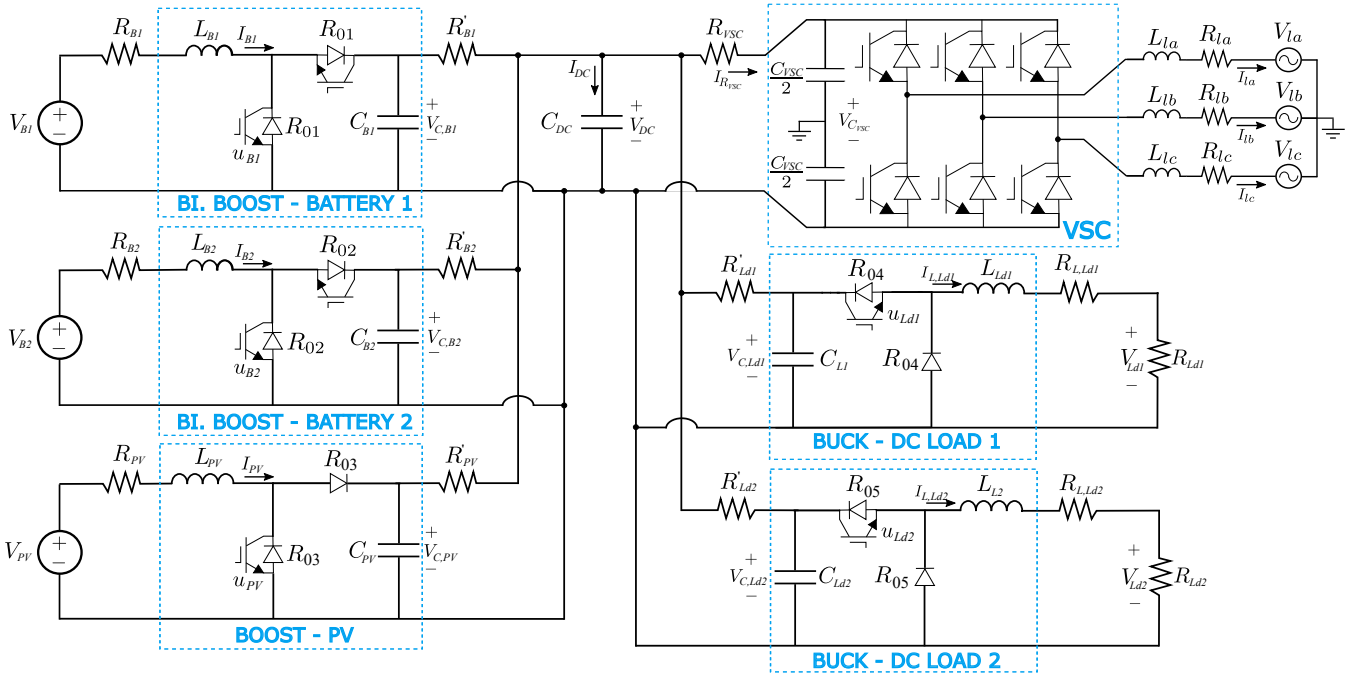

Fig. 2: Electrical circuit of the considered DC Microgrid setup

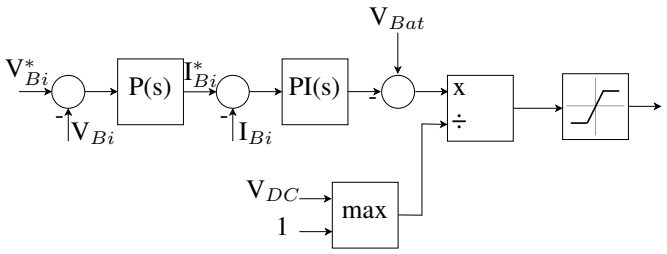

Fig. 3: Cascaded Proportional-Integral control scheme

where $\mathcal{L}_{g_i}$, $\mathcal{L}^1_{f_i}$ and $\mathcal{L}^2_{f_i}$ are the Lie derivatives of $V_{C,Bi}$ computed as:

$$\mathcal{L}^2_{f_i} = \frac{\dot{V}_{DC}}{R'_{Bi}C_{Bi}} - \frac{1}{R'_{Bi}C_{Bi}}\dot{V}_{C,Bi} + -\frac{I^*_{Bi}}{C_{Bi}V^2_{C,Bi}}\left(V_{Bi} - (R_{Bi}+R_{0i})I^*_{Bi}\right)\dot{V}_{C,Bi} \quad (8)$$

$$\mathcal{L}_{g_i}\mathcal{L}^1_{f_i}(V_{C,Bi}) = \frac{1}{C_{Bi}V_{C,Bi}}\left(V_{Bi} - 2(R_{Bi}+R_{0i})I^*_{Bi}\right) \quad (9)$$

The current reference is calculated by integrating (7). An additional control input v_d is included to set new desired dynamics for $V_{C,Bi}$:

$$v_d = -K_i(\dot{V}_{C,Bi} - \dot{V}^*_{DC}) - K^\alpha_i(V_{C,Bi} - V^*_{DC}) \quad (10)$$

Subsequently, the closed loop of the resulting linear second-order system is written as:

$$\begin{bmatrix} \dot{V}_{C,Bi} \\ \ddot{V}_{C,Bi} \end{bmatrix} = \begin{bmatrix} 0 & 1 \\ -K^\alpha_i & -K_i \end{bmatrix} \begin{bmatrix} V_{C,Bi} - V^*_{DC} \\ \dot{V}_{C,Bi} - \dot{V}^*_{DC} \end{bmatrix} \quad (11)$$

Therefore, in (11) a linear second-order system is obtained referring to the closed-loop function of the voltage control in the batteries.

The resulting nonlinear controller can be compared to a PD controller from linear control design, as it implements a proportional and a derivative action to improve the control performance. The great advantage of this approach is the power sharing capability for multiple battery devices, *e.g.* both batteries can control their respective output voltages independently without control conflict because no integral term is used to control the voltage.

2) Control of the VSC: The three-phase VSC is controlled with a grid following control, using a synchronous reference frame phase locked loop (PLL) [25]. The three-phase voltages V_{abc} are mapped to the $dq0$-frame, with the q-axis voltage V_q acting as the input to the PI controller.

$$u_d = \frac{2}{V_{dc}}\left[L_l\phi_d + R_l I_{l,d} - \omega L_l I_{l,q} + V_{l,d}\right] \quad (12)$$

$$u_q = \frac{2}{V_{dc}}\left[L_l\phi_q + R_l I_{l,q} + \omega L_l I_{l,d} + V_{l,q}\right] \quad (13)$$

where u_{dq} are the control inputs and ϕ_{dq} is the PI controller.

$$\phi_{dq} = -K_{dq}(I_{l,dq} - I^*_{l,dq}) - K^\alpha_{dq}\alpha_{dq} \quad (14)$$

$$\dot{\alpha}_{dq} = I_{l,dq} - I^*_{l,dq} \quad (15)$$

Therefore, a linear subspace is obtained, assuring the stability for this subsystem.

By assuming a power factor, the active and reactive power on the AC side can be treated decoupled and the reference currents i^*_{ld} and i^*_{lq} can be chosen as [26]:

$$i^*_{ld} = \frac{2}{3}\frac{P^*_{VSC}}{V_{ld}} \quad (16)$$

$$i_{lq}^{*} = -\frac{2}{3}\frac{Q_{VSC}^{*}}{V_{ld}} \tag{17}$$

with P_{VSC}^{*} and Q_{VSC}^{*} as the reference values for active and reactive power at the VSC output. V_{ld} is the direct component of the output voltage at the VSC.

IV. Experimental PHIL-Setup

This section introduce the experimental PHIL setup of the AC-connected DC Microgrid. An electrical circuit diagram of the DC Microgrid is shown in Fig. 2 The PHIL system includes physical circuits realized by silicon carbide (SiC) MOSFETs. The switching frequency is chosen to be 20 kHz, which seems to be a good compromise between dynamics and efficiency[1]. The PV emulator system emulates a polycrystalline IBC Solar PolySol with a nominal power of 3 kWp, an open circuit voltage of $V_{OC} = 351.0\,\mathrm{V}$ and a short circuit current of $I_{SC} = 8\,\mathrm{A}$. The control algorithms are implemented in a real-time rapid prototyping system from Imperix[2] The experimental setup is depicted in Fig. 4, while component parameters are

Fig. 4: Real-time PHIL setup consisting of PV emulator, loads, Real-time controller, SiC-MOSFETs, passive components and battery emulator

listed in Tab. I.

TABLE I: Microgrid parameters

Battery 1	Battery 2	PV	Load 1	Load 2	Value
R_{B1}	R_{B2}	R_{PV}	R_{L1}	R_{L2}	0.1 Ω
C_{B1}	C_{B2}	C_{PV}	C_{L1}	C_{L2}	$500\mu F$
R'_{B1}	R'_{B2}	R'_{PV}	R'_{L1}	R'_{L2}	0.1 Ω
L_{B1}	L_{B2}	L_{PV}	L_{L1}	L_{L2}	2.5 mH
R_{01}	R_{02}	R_{03}	R_{04}	R_{05}	10 $m\Omega$

[1]High frequency = smaller size, faster transient response and smaller voltage overshoot and undershoot, but increased losses and heat and also more EMV problems.

[2]https://imperix.com/products/control/rapid-prototyping-controller/

V. Experimental results

This section presents experimental results from applying the proposed nonlinear control method to a PHIL setup. The control parameters used for the experiments are listed in Tab. II. In the experiments, the DC Microgrid was first brought to

TABLE II: Control parameters

$\mathbf{K_{P,VBi}}$	$\mathbf{K_{I,VBi}}$	$\mathbf{K_{P,IBi}}$	$\mathbf{K_{I,IBi}}$
0.1	5	0.01	0.1
$\mathbf{K_{Bi}}$	$\mathbf{K_{Bi}^{\alpha}}$	$\mathbf{K_{i}}$	$\mathbf{K_{i}^{\alpha}}$
1000	25000	400	0.2
$\mathbf{K_{p,d}}$	$\mathbf{K_{i,d}}$	$\mathbf{K_{p,q}}$	$\mathbf{K_{i,q}}$
50	100	50	100

its steady state by gradually increasing the reference values to mitigate inrush currents. Due to its minor importance, this part is not shown in the figures. To ensure a consistent comparison of both control approaches, the influence of weather changes on the PV emulator system is excluded by generally setting the irradiance to 0 $\mathrm{W/m^2}$ in general. In Fig. 5, a DC Microgrid with one battery in isolated mode is excited by a load step of $\Delta P_{Ld1} = 2$ kW at $t = 0.5s$. The first subplot shows that the DC voltage ripple is more pronounced for the PI-based control (blue) than for the nonlinear control (orange). The significant drop in the load voltage in the second subplot is attributable to the lack of capacitance on the load side. The third and fourth subplots illustrate the increased rise in load power and load currents. In Fig. 6 the results using a cascaded PI and those using the proposed nonlinear control are shown for an isolated DC Microgrid with two batteries and the same load step of $\Delta P_{Ld1} = 2$ kW at $t = 0.5s$. As can be seen from the first subplot, the voltage drop is lower when the nonlinear control (orange) is used as opposed to the PI-based control (blue). For the second to fourth subplots, the same applies as before in Fig. 5. The case of a grid-connected DC Microgrid with two batteries is shown in Fig. 7. Here, at $t = 05.s$, a reference power of $P = 3\,\mathrm{kW}$ is supplied to the voltage source converter. As indicated in the first subplot, the nonlinear control (orange) achieves a reduced drop in the DC voltage V_{DC} compared to the PI-based control (blue). The second plot shows the performance of the batteries. It is noticeable that in the case of the PI-based controller (blue and orange), the two battery output powers are closer together, resulting in better load-sharing compared to the nonlinear controlled (yellow and purple) DC Microgrid. The third subplot shows the power step on the VSC.

VI. Conclusion

In the present paper, the authors extend the application of nonlinear control methods to enhance the grid-connecting capability of power systems utilizing multiple batteries. The performance of the extended nonlinear control method is compared to a conventional PI-based control strategy through implementation on a PHIL system. Our findings reveal that the extended nonlinear control demonstrates notable improvements in voltage maintenance compared to the PI-based control. This enhancement is particularly significant for ensur-

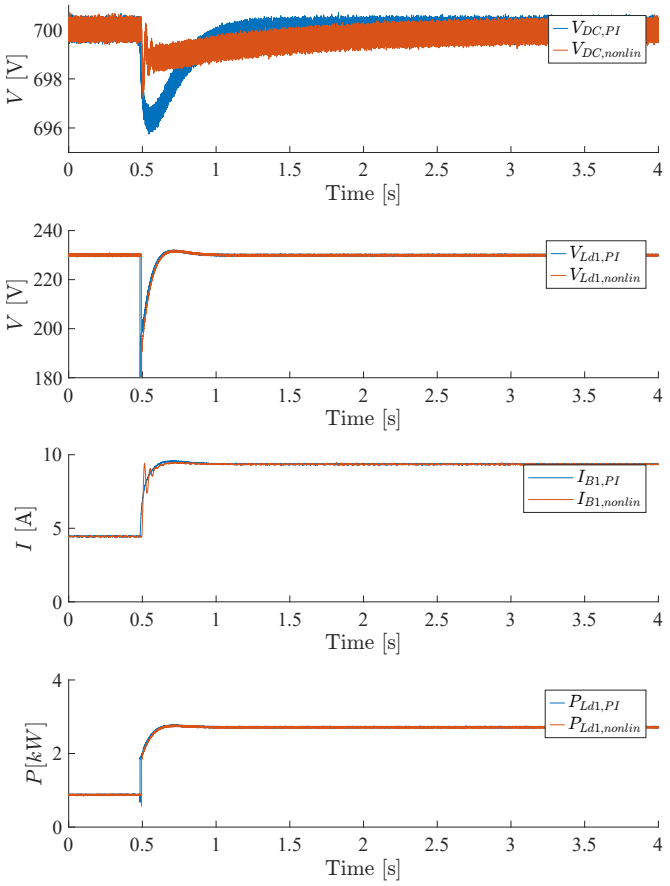

Fig. 5: PI and nonlinear controlled DC Microgrid voltage, load's voltage, current and controller duty cycle during a load step at $t = 0.5s$ with only one battery in isolated mode.

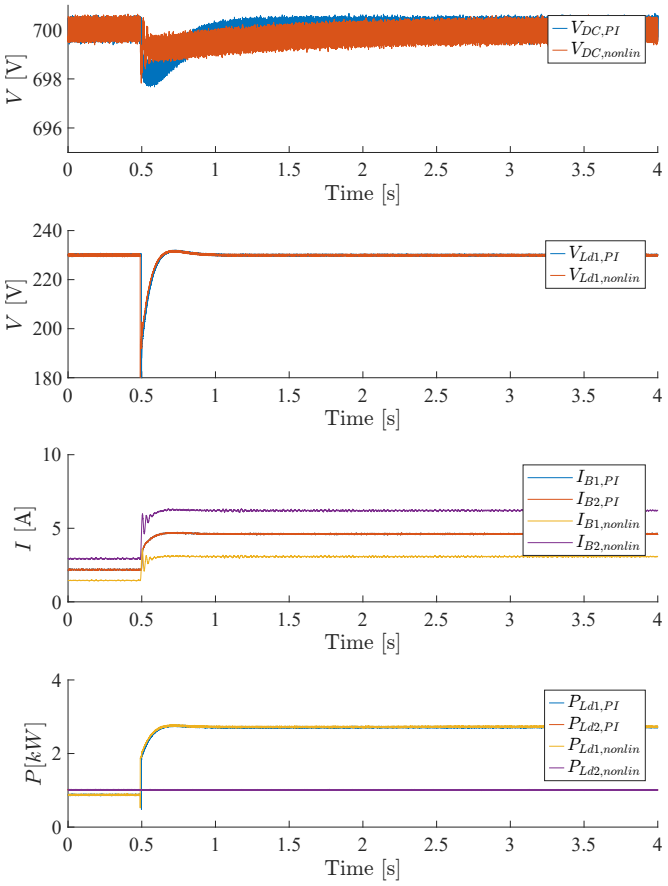

Fig. 6: PI and nonlinear controlled DC Microgrid voltage, load's voltage, current and controller duty cycle during a load step at $t = 0.5s$ with two batteries in isolated mode.

ing system stability and reliability, which are crucial issues in modern power systems. However, our investigation also reveals a trade-off, as the nonlinear control exhibits reduced load-sharing capabilities compared to the PI-based approach. The observed improvement in voltage maintenance underscores the potential of nonlinear control methods to address critical challenges in grid-connected power systems, particularly in scenarios involving multiple energy storage units. By effectively regulating voltage levels, extended nonlinear control helps to improve system performance and resilience to disturbances.

However, the identified trade-off between voltage maintenance and load-sharing capability highlights the importance of considering different system requirements and operational objectives in controller design. While prioritizing voltage stability is essential, future research should explore methods to mitigate the impact on load-sharing, to ensure a balanced approach to system optimization. It is important to acknowledge certain limitations of our study, including the specific conditions of the implemented PHIL system and the simplifications made in modeling and simulation. Future research efforts should address these limitations by conducting experiments under varied operating conditions and incorporating more comprehensive system models. In addition, the exploration of advanced control techniques and optimization algorithms may provide avenues to further improve the performance and robustness of grid-connected power systems.

In conclusion, the study demonstrates the effectiveness of extending nonlinear control methods to improve voltage maintenance in grid-connected power systems with multiple batteries. While acknowledging the trade-offs inherent in controller design, our results underscore the potential of nonlinear control approaches to address some key challenges in modern power systems.

REFERENCES

[1] A. Sauer, *The DC-factory*. Hanser eLibrary, München: Hanser, [2021].

[2] J. J. Justo, F. Mwasilu, J. Lee, and J.-W. Jung, "AC-microgrids versus DC-microgrids with distributed energy resources: A review," *Renewable and sustainable energy reviews*, vol. 24, pp. 387–405, 2013.

[3] A. T. Elsayed, A. A. Mohamed, and O. A. Mohammed, "DC microgrids and distribution systems: An overview," *Electric power systems research*, vol. 119, pp. 407–417, 2015.

[4] Ö. Ekin, F. Perez, G. Damm, and V. Hagenmeyer, "A real-time PHIL implementation of a novel nonlinear distributed control strategy for a multi-terminal DC microgrid," in *2023 IEEE Belgrade PowerTech*, pp. 1–6, 2023.

[5] F. Perez and G. Damm, "DC microgrids," in *Microgrids design and implementation*, pp. 447–475, 2019.

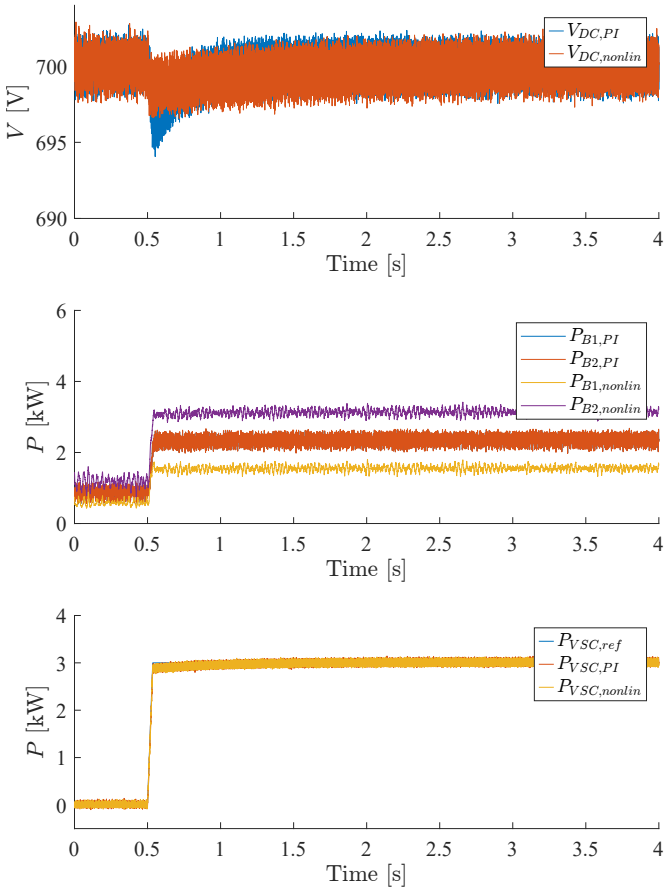

Fig. 7: PI and nonlinear controlled DC Microgrid voltage, load's voltage, current and controller duty cycle during a load step at $t = 0.5s$ with two batteries in grid-connected mode.

[6] S. Sen and V. Kumar, "Microgrid control: A comprehensive survey," *Annual Reviews in control*, vol. 45, pp. 118–151, 2018.

[7] D. I. Makrygiorgou and A. T. Alexandridis, "Stability analysis of dc distribution systems with droop-based charge sharing on energy storage devices," *Energies*, vol. 10, no. 4, p. 433, 2017.

[8] Q. Guo, M. J. Carrizosa, A. Iovine, and A. Arzandé, "Dynamic feedback linearization and singular perturbation for a stabilizing controller for DC/DC boost converters: theory and experimental validation," *IEEE Transactions on Industrial Electronics*, 2023.

[9] F. Perez, G. Damm, F. Lamnabhi-Lagarrigue, and P. Ribeiro, "Nonlinear control for isolated DC microgrids," *Revue Africaine de la Recherche en Informatique et Mathématiques Appliquées*, vol. Volume 30 - 2019 - MADEV..., 05 2018.

[10] A. Emadi, A. Khaligh, C. Rivetta, and G. Williamson, "Constant power loads and negative impedance instability in automotive systems: definition, modeling, stability, and control of power electronic converters and motor drives," *IEEE Transactions on Vehicular Technology*, vol. 55, no. 4, pp. 1112–1125, 2006.

[11] M. Jiménez Carrizosa, A. Iovine, G. Damm, and P. Alou, "Droop-inspired nonlinear control of a DC microgrid for integration of electrical mobility providing ancillary services to the AC main grid," *IEEE Transactions on Smart Grid*, vol. 13, no. 5, pp. 4113–4122, 2022.

[12] N. Yang, B. Nahid-Mobarakeh, F. Gao, D. Paire, A. Miraoui, and W. Liu, "Modeling and stability analysis of multi-time scale DC microgrid," *Electric Power Systems Research*, vol. 140, pp. 906–916, 2016.

[13] J. Ferguson, M. Cucuzzella, and J. M. Scherpen, "Exponential stability and local ISS for DC networks," *IEEE Control Systems Letters*, vol. 5, no. 3, pp. 893–898, 2020.

[14] G. Lin, J. Liu, C. Rehtanz, Y. Li, W. Zuo, and P. Wang, "Analysis of instability causes in the bi-DC converter and enhancing its performance by improving the damping in the IDA-PBC control," *IET Generation, Transmission & Distribution*, vol. 15, no. 17, pp. 2411–2421, 2021.

[15] S. M. Azimi and M. Hamzeh, "Voltage/current large transient suppression in DC microgrids using local information and active stabilizing capability," *IEEE Systems Journal*, vol. 14, no. 1, pp. 1109–1116, 2019.

[16] A. Salazar, A. Berzoy, and J. M. Velni, "Nonlinear control design for bidirectional synchronous buck-boost converters used in residential battery storage systems," in *2019 IEEE Energy Conversion Congress and Exposition (ECCE)*, pp. 2485–2490, IEEE, 2019.

[17] J. W. Kimball and P. T. Krein, "Singular perturbation theory for DC–DC converters and application to pfc converters," *IEEE Transactions on Power Electronics*, vol. 23, no. 6, pp. 2970–2981, 2008.

[18] K. Gajula, L. K. Marepalli, and L. Herrera, "Approximate sensitivity conditioning and singular perturbation analysis for power converters," *arXiv preprint arXiv:2203.16811*, 2022.

[19] F. Perez, G. Damm, and P. Ribeiro, *DC Microgrids for Ancillary Services Provision*, pp. 403–437. Cham: Springer International Publishing, 2022.

[20] F. Perez, A. Iovine, G. Damm, L. Galai-Dol, and P. F. Ribeiro, "Stability analysis of a DC microgrid for a smart railway station integrating renewable sources," *IEEE Transactions on Control Systems Technology*, 2019.

[21] D. Sera, L. Mathe, T. Kerekes, S. V. Spataru, and R. Teodorescu, "On the perturb-and-observe and incremental conductance mppt methods for PV systems," *IEEE Journal of Photovoltaics*, vol. 3, pp. 1070–1078, 2013.

[22] D. C. Huynh and M. W. Dunnigan, "Development and comparison of an improved incremental conductance algorithm for tracking the mpp of a solar PV panel," *IEEE Transactions on Sustainable Energy*, vol. 7, no. 4, pp. 1421–1429, 2016.

[23] F. Wiegel, J. Wachter, M. Kyesswa, R. Mikut, S. Waczowicz, and V. Hagenmeyer, "Smart energy system control laboratory – a fully-automated and user-oriented research infrastructure for controlling and operating smart energy systems," *at - Automatisierungstechnik*, vol. 70, pp. 1116 – 1133, 2022.

[24] K. Åström and T. Hägglund, *Advanced PID Control*. ISA - The Instrumentation, Systems and Automation Society, 2006.

[25] S.-K. Chung, "A phase tracking system for three phase utility interface inverters," *IEEE Transactions on Power Electronics*, vol. 15, no. 3, pp. 431–438, 2000.

[26] P. Kundur, N. Balu, and M. Lauby, *Power System Stability and Control*. EPRI power system engineering series, McGraw-Hill, 1994.